RESEARCH ARTICLE | JANUARY 29 2025

Squeezed microwave and magnonic frequency combs

A. Kani; M. Hatifi ; J. Twamley

APL Quantum 2, 016112 (2025)
https://doi.org/10.1063/5.0245193

Squeezed microwave and magnonic frequency combs

Cite as: APL Quantum 2, 016112 (2025); doi: 10.1063/5.0245193
Submitted: 24 October 2024 • Accepted: 13 January 2025 •
Published Online: 29 January 2025

A. Kani,[a] M. Hatifi,[b] and J. Twamley[c]

AFFILIATIONS

Quantum Machines Unit, Okinawa Institute of Science and Technology Graduate University, Okinawa 904-0495, Japan

[a]**New affiliation**: School of Physics, University of Hyderabad, Hyderabad, Telangana 500046, India
[b]**New affiliation**: Aix Marseille Univ, CNRS, Centrale Med, Institut Fresnel, UMR 7249, 13397 Marseille, France
[c]**Author to whom correspondence should be addressed:** jason.twamley@oist.jp

ABSTRACT

We present a theoretical framework for generating squeezed microwave and magnonic frequency combs achieved through the parametric coupling of magnon modes to a cavity. This coupling exploits the intrinsic non-linear magnon modes of a ferromagnetic sphere. When subjected to a strong, coherent microwave field, we show that the system exhibits spontaneous generation of squeezed frequency combs. Our exploration crosses various regimes of comb generation, prominently highlighting phenomena such as squeezing and squeezed lasing. This study paves the way for a pioneering room-temperature, multi-frequency maser characterized by both its magnonic and microwave squeezing properties. The implications of our findings hold promise for advancements in spintronics, quantum sensing, information processing, and quantum networking.

INTRODUCTION

Microwave cavity-magnonics emerges as a powerful platform for continuous-variable quantum computing and quantum information processing due to its strong coupling between magnons in a large ferromagnetic crystal and microwave cavity photons.[1–8] This strong interaction sets the stage for efficient transfer and fast operation of quantum information. High-fidelity quantum information processing fundamentally relies on the generation of nonclassical states.[9,10] Realizing such states involves exploiting strong nonlinearities. In the optical realm, optical parametric coupling has played a major role in quantum engineering endeavors.[11–17] Optical frequency combs (FCs),[18,19] squeezed laser,[20] and squeezed optical frequency combs[13] have gained recognition as formidable tools for precision metrology and spectroscopy, positioning themselves as strong contenders for quantum processing.[21–24]

The landscape of frequency comb (FC) research has seen a rich tapestry of studies delving into nonlinear processes, unveiling techniques for generating bosonic FCs.[13–17,25–31] Of particular interest in the emergence of magnonic quantum computing is the generation of quantum magnonic frequency combs (FCs). The generation of magnonic FCs is demonstrated by leveraging intrinsic magnon nonlinearity and various nonlinear magnon scattering processes[32–36] or through the use of nonlinearly coupled hybrid magnonic systems.[37–40] However, while promising, the generation of squeezed magnons often faces challenges tied to the necessity of strong magnon nonlinearity[41] or a squeezed microwave source.[42,43] Standard sources of magnonic FCs[32–40] are incompatible with the generation and control of squeezing. Recognizing these hurdles, our work proposes a novel theoretical framework for parametric cavity–magnon coupling, offering efficient generation of squeezed magnons and squeezed magnonic FCs. Squeezed magnons find potential applications in enhanced ground state cooling of macroscopic mechanical systems,[44] increased entanglement,[45] and microwave storage.[46] Squeezed magnonic FCs offer promising prospects in continuous-variable quantum computing[9,10] and multiplexed quantum networks.[47] Besides the generation of squeezed magnons, our system produces squeezed microwaves and squeezed microwave FCs, presenting significant opportunities in high-precision sensing, magnetic resonance imaging,[48] and communication[49] and serving as a nonclassical source for superconducting quantum computing.[50,51]

Historically, the parametric excitation of magnons has been extensively studied and has proven crucial in generating and amplifying spin waves.[52–55] In open geometries, this process typically results in pairs of coherent spin waves propagating in opposite directions.[56] Diverging from this standard paradigm, we focus on coupling a ferromagnet's magnetostatic modes to a cavity's standing mode. This coupling is anchored in the noncircular precessional motion of spins, giving rise to novel nonlinear energy exchange processes.[57–61] While conventional cavity–magnon studies have been limited to the Kittel magnon mode, we explore the broader spectrum of magnon modes present in a spherical ferromagnet. By harnessing this broader understanding, we unveil new avenues for parametric cavity–magnon coupling. This coupled system driven by a strong coherent microwave field leads to the spontaneous generation of squeezed microwave and magnonic FCs. Beyond just generation, our approach offers unparalleled control over these FCs.

NONLINEAR PARAMETRIC CAVITY–MAGNON INTERACTION

We consider a single crystalline sphere of yttrium iron garnet—$Y_3Fe_5O_{12}$ (YIG),[62] an excellent magnonic system that is uniformly magnetized to its saturation value M_s along the z-direction by applying a large bias magnetic field $H_0\boldsymbol{e}_z > M_s\boldsymbol{e}_z/3$ and placed inside a microwave cavity, as shown in Fig. 1. In a spherical crystal, an infinite number of magnon modes exist,[63] and each mode is characterized by three indices (n, l, q), where n is an integer, m is the azimuthal wave number with $m \in [-n, n]$, and the third index q takes values from 0 to $q_{\max}(n, m)$ depending on the number of allowed modes for each (n, m).[64] These three indices collectively determine the frequency and spatial structure of the magnon mode. A YIG sphere supports many high-Q magnon modes with damping rates ~MHz.[65,66] The discrete nature with differing spatial mode structures allows us to focus on any particular magnon mode.[65–68] Let us assume that the total induced magnetization of the YIG sphere has a magnitude $\|\hat{\boldsymbol{M}}\| = M_S$, which is mostly along the $\boldsymbol{e}_z$ direction, the direction of the bias magnetic field. Due to the conservation of angular momentum, the magnetization of the sphere retains this magnitude even when it is slightly rotated or precessing. Letting $\hat{\boldsymbol{m}}$ be the magnetization operator for the spin wave mode, which is typically very small, $\langle|\hat{\boldsymbol{m}}|\rangle \ll M_s$, and lies in the xy-plane, we can write $\hat{\boldsymbol{M}} = \hat{\boldsymbol{m}} + m_z\hat{\boldsymbol{e}}_z$. Since $M_S^2 = \hat{\boldsymbol{m}}\cdot\hat{\boldsymbol{m}} + m_z^2$, we can express the total magnetization in terms of only M_S and $\hat{\boldsymbol{m}}$ as

$$\hat{\boldsymbol{M}} = \hat{\boldsymbol{m}} + \sqrt{M_s^2 - \hat{\boldsymbol{m}}\cdot\hat{\boldsymbol{m}}}\,\boldsymbol{e}_z \approx \hat{\boldsymbol{m}} + \left(M_s\mathbb{I} - \frac{\hat{\boldsymbol{m}}\cdot\hat{\boldsymbol{m}}}{2M_s}\right)\boldsymbol{e}_z. \tag{1}$$

The nonlinearity in the z component is necessary to correctly define the magnitude of the total magnetization.[60,69] The spin wave magnetization couples to the cavity field through the magnetic dipole interaction $\hat{\boldsymbol{H}}_{\text{int}} = -\int\hat{\boldsymbol{M}}\cdot\hat{\boldsymbol{B}}\,dV$, where $\hat{\boldsymbol{B}}$ is the cavity magnetic field. Within the spin wave approximation ($\langle|\hat{\boldsymbol{m}}|\rangle \ll M_s$), $\hat{\boldsymbol{m}}$ is confined on the x–y plane.[64] Conventionally, one uses a cavity mode whose magnetic field is polarized in the x–y plane to directly couple the magnon modes.[6–8] This direct cavity–magnon coupling is strong but linear. As seen from Eq. (1), the magnons can be coupled nonlinearly to the z-component of the microwave field. There are magnon modes, namely orbital angular momentum eigenmodes, where the collective spins precess circularly about the z-axis.[70] Such circularly precessing magnon modes have no dynamics with respect to their projection onto their z-component, making the excitation of these modes difficult by z-polarized time-varying magnetic fields (microwaves). Interestingly, most of the magnon modes of a spherical ferromagnet are hybrid orbital angular momentum modes and noncircular precessing modes. Such a motion of spins modulates the longitudinal component of the magnetization that can be parametrically coupled to the microwave field at a frequency twice the magnon frequency. Here, we focus on the lowest order noncircular precessing magnon mode, namely the (2,0,0) mode,[64,71,72] which can be excited via the application of a non-uniform magnetic field and can be selectively addressed via tuning the cavity mode to the mode's specific frequency, as shown in previous experimental studies.[71,72] The (2,0,0) magnetization precession can be written as

$$\hat{\boldsymbol{m}} = \frac{M_0}{R\sqrt{\omega_s\omega_0}}\left((\omega_0 x - i\omega_s y)\boldsymbol{e}_x + (i\omega_s x + \omega_0 y)\boldsymbol{e}_y\right)\hat{\boldsymbol{s}} + H.c., \tag{2}$$

where $\hat{\boldsymbol{s}}$ is the magnonic annihilation operator, $M_0 = \sqrt{(5\gamma\hbar M_s)/(4V)}$ is the zero-point magnetization, γ is the gyromagnetic ratio, $\omega_s = \sqrt{\omega_0(\omega_0 + 4\mu_0\gamma M_s/5)}$ is the resonance frequency of the magnon mode, $\omega_0 = \gamma\mu_0(H_0 - M_s/3)$, and R and V are the radius and volume of the sphere, respectively. Considering the cavity magnetic field to be polarized along the z axis and placing a small YIG sphere with $R \ll \lambda$, where λ is the wavelength of the cavity field, at the antinode of the cavity magnetic field, we can write $\hat{\boldsymbol{B}} = iB_0\boldsymbol{e}_z(\hat{\boldsymbol{a}}^\dagger - \hat{\boldsymbol{a}})$, where $\hat{\boldsymbol{a}}$ is the annihilation operator of the cavity mode, $B_0 = \sqrt{\frac{\mu_0\omega_a\hbar}{2V_c}}$ is the zero-point magnetic field, ω_a is the resonance frequency of the cavity, and V_c is the cavity volume; the cavity–magnon interaction is given by $\hat{\boldsymbol{H}}_{\text{int}} = -\int\hat{\boldsymbol{M}}\cdot\hat{\boldsymbol{B}}\,dV \equiv \int U\,dV$. Using the expression for the total magnetization from Eq. (1), where the spin-wave mode is expressed as Eq. (2), and taking the cavity

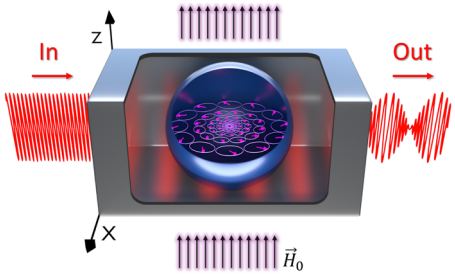

FIG. 1. Schematic of the system: a spherical ferromagnetic insulator is placed inside a microwave cavity. The sphere is uniformly magnetized to saturation magnetization along the z axis by a homogeneous bias magnetic field $\mu_0 H_0\mathbf{e}_z$ and placed at the maximum of the cavity B_z. For this study, we specifically chose to excite the noncircular precessing magnon mode (2,0,0) and make it interact with the cavity through its magnetic field B_z.

magnetic field as above, we can evaluate the integrand U involving the magnon operators as

$$U = \frac{iB_0M_0^2}{2M_s\omega_0\omega_s R^2}(\hat{\boldsymbol{a}} - \hat{\boldsymbol{a}}^\dagger) \times \left[\omega_s^2(\hat{\boldsymbol{s}} - \hat{\boldsymbol{s}}^\dagger)^2 - \omega_0^2(\hat{\boldsymbol{s}} + \hat{\boldsymbol{s}}^\dagger)^2\right](x^2 + y^2). \tag{3}$$

One can now perform the volume integral over the YIG sphere of radius R to obtain

$$\hat{\boldsymbol{H}}_{\rm int} = \frac{iVB_0M_0^2}{5M_s\omega_s\omega_0}(\hat{\boldsymbol{a}} - \hat{\boldsymbol{a}}^\dagger) \times \left[\omega_s^2(\hat{\boldsymbol{s}} - \hat{\boldsymbol{s}}^\dagger)^2 - \omega_0^2(\hat{\boldsymbol{s}} + \hat{\boldsymbol{s}}^\dagger)^2\right], \tag{4}$$

where V is the volume of the sphere. The magnetization modulation caused by the noncircular precessional motion can be made to interact efficiently by considering the cavity frequency ω_a to be nearly twice the magnon frequency, $\omega_a \approx 2\omega_s$.[60,73] When the cavity–magnon coupling strength is not in the deep strong limit $(\leq \omega_s, \omega_a)$ and by undertaking a rotating wave approximation, one can approximate the above interaction Hamiltonian to be of the form

$$\hat{\boldsymbol{H}}_{\rm int} = iVB_0\frac{M_0^2}{5M_s\omega_s\omega_0}(\omega_s^2 - \omega_0^2)(\hat{\boldsymbol{a}}\hat{\boldsymbol{s}}^{\dagger 2} - \hat{\boldsymbol{a}}^\dagger\hat{\boldsymbol{s}}^2) = i\hbar g(\hat{\boldsymbol{a}}\hat{\boldsymbol{s}}^{\dagger 2} - \hat{\boldsymbol{a}}^\dagger\hat{\boldsymbol{s}}^2), \tag{5}$$

where g is the parametric cavity–magnon coupling strength. Near the subharmonic resonance $\omega_a = 2\omega_s$, $g = \frac{\sqrt{2}}{5}\gamma^2\mu_0 M_s\sqrt{\frac{\mu_0\hbar}{\omega_a V_c}}$, which is independent of the particle size. For a YIG sphere ($M_s = 5.87 \times 10^5$ Am^{-1} and $\gamma = 2\pi \times 28$ GHz),[69] in a microwave cavity of dimension $V_c \sim 1$ cm^3 supporting a frequency of $\omega_a = 2\pi \times 10$ GHz,[8] the nonlinear cavity–magnon coupling strength $g \approx 2\pi \times 0.047$ Hz. This parametric coupling strength is nine orders larger than the intrinsic Kerr nonlinearity in an mm-sized YIG sphere,[41,74–76] making the nonlinear Kerr effect negligible. We study the nonlinear response of the system by driving the cavity mode at the frequency $\omega_d \approx \omega_a \approx 2\omega_s$. The total Hamiltonian of the driven cavity-magnonic system is

$$\hat{\boldsymbol{H}}/\hbar = \omega_a\hat{\boldsymbol{a}}^\dagger\hat{\boldsymbol{a}} + \omega_s\hat{\boldsymbol{s}}^\dagger\hat{\boldsymbol{s}} + ig(\hat{\boldsymbol{a}}\hat{\boldsymbol{s}}^{\dagger 2} - \hat{\boldsymbol{a}}^\dagger\hat{\boldsymbol{s}}^2) + if_a\left(\hat{\boldsymbol{a}}^\dagger e^{-i\omega_d t} - \hat{\boldsymbol{a}}e^{i\omega_d t}\right), \tag{6}$$

where f_a is the microwave cavity drive amplitude related to the input microwave power P and the cavity damping rate γ_a ~MHz[7] by $f_a = \sqrt{P\gamma_a/\hbar\omega_a}$. The dynamics of the system are then described by the semiclassical nonlinear Langevin equations,[77–79]

$$\begin{aligned}\dot{a} &= -\left(\frac{\gamma_a}{2} - i\Delta_a\right)a - g\,s^2 + f_a + \sqrt{\gamma_a}\xi_a(t),\\ \dot{s} &= -\left(\frac{\gamma_s}{2} - i\Delta_s\right)s + 2g\,as^* + \sqrt{\gamma_s}\xi_s(t),\end{aligned} \tag{7}$$

where $\Delta_a = \omega_d - \omega_a$, $\Delta_s = \frac{\omega_d}{2} - \omega_s$, γ_s is the magnon damping rate, ξ_j is the stochastic noise operator describing the thermal distribution of the mode $j \in a, s$ with the mean thermal occupancy $\bar{n}_j$ that obeys the quantum correlations $\langle\xi_j(t)\rangle = 0$, $\langle\xi_j(t)\xi_j^\dagger(t')\rangle = (\bar{n}_j + 1)\,\delta(t - t')$, and $\langle\xi_j^\dagger(t)\xi_j(t')\rangle = \bar{n}_j\delta(t - t')$. The damping rate of the (2,0,0) magnon mode in a large mm-sized YIG sphere is ~MHz.[71]

At room temperature, $\bar{n}_a(\omega_a = 10\,\text{GHz}) \approx 625$ and $\bar{n}_s(\omega_s = 5\,\text{GHz}) \approx 1250$.

ANALYSIS OF MASER AND COMB PROPERTIES

First, we study the mean dynamics of the system. In the absence of noise, the drive-microwave-power-dependent spectral response, which is the fast Fourier transforms (FFTs) of the mean cavity–magnon dynamics, in the long timescale is shown in Fig. 2. This consists of three distinct regions separated by two different values of the threshold drive power. Above a certain threshold of drive power $f_a > f_a^{lase}$, the amplitude of the cavity field saturates and the magnon mode starts to lase at a frequency equal to half the drive frequency. This is shown by the lower dashed line in Fig. 2. Further increasing the power for a specific range of detunings, another drive power threshold exists, $f_a > f_a^{comb}$, beyond which the dynamics of both the cavity and the magnon modes are nonsinusoidal, consisting of multiple equally spaced frequencies.

We now investigate the generation of this FC. When the drive field strength is below the FC threshold $f_a < f_a^{comb}$, we linearize the Langevin equation [Eq. (7)] around the mean steady-state constant-amplitude response and completely characterize the dynamics of the system. The steady-state noise power spectral density $S_{c^\dagger c}(\omega) = \int c^\dagger(\omega)c(\omega')d\omega'$, where $c = (a, s)$, is obtained by solving the linearized Langevin equation in the frequency domain, and these spectra are shown in Fig. 3. At low powers, from Fig. 3(a), we observe that the cavity noise spectrum is unaffected. In contrast, from Fig. 3(b), the coherent cavity photon driving of the two-magnon transition pulls the resonance frequency of the magnon mode toward $\omega_s = \omega_d/2$ and narrows the spectral line. Eventually, the spectral linewidth goes to zero at the drive power threshold $f_a \equiv f_a^{lase}$, where

$$f_a^{lase} = \frac{\sqrt{(\gamma_a^2 + 4\Delta_a^2)(\gamma_s^2 + 4\Delta_s^2)}}{8g}, \tag{8}$$

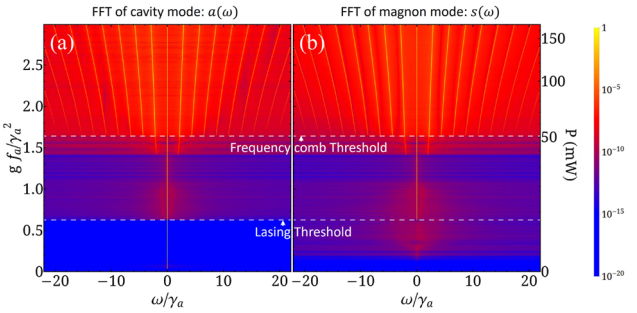

FIG. 2. Cavity-magnonic FC generation: the FFTs of the cavity (left) and magnon (right) modes. (a) FFT of the rescaled cavity mode $\frac{g}{\gamma_a}a(\omega)$ and (b) FFT of the rescaled magnon mode $\frac{g}{\gamma_a}s(\omega)$, as a function of the input power (left axis labeled in $g\,f_a/\gamma_a^2$ and right axis labeled in mW) and as a function of frequency ω/γ_a. The dashed lines in both figures represent the threshold drive values (f_a^{lase}, f_a^{comb}), where phase transitions occur, as defined by Eqs. (8) and (9), respectively. Here, we chose the following parameters: $(\gamma_a, \gamma_s, \Delta_a, \Delta_s)/2\pi = (1, 1, -1, 1)$ MHz and $g = 2\pi \times 0.047$ Hz.

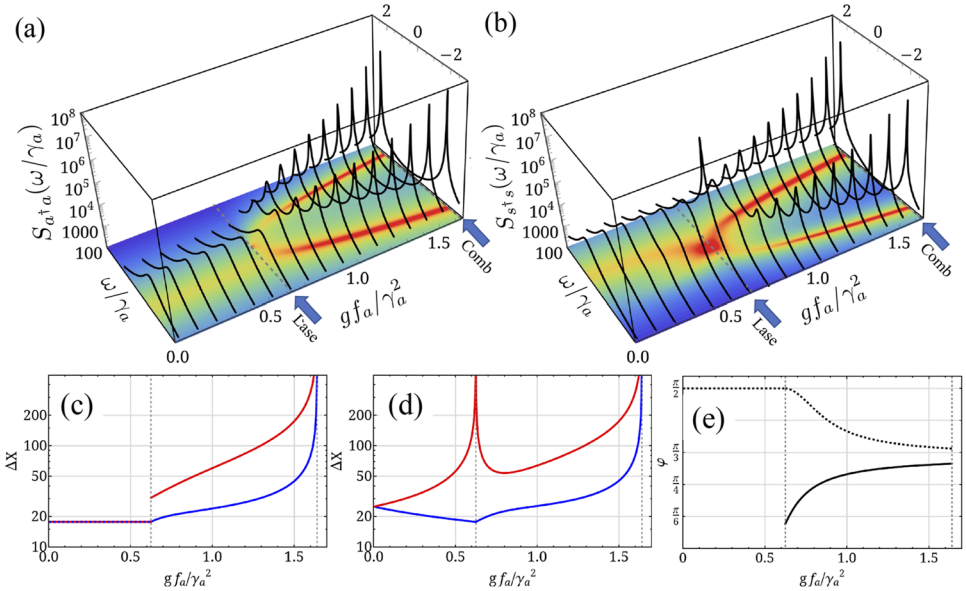

FIG. 3. Noise power spectral density: the drive amplitude-dependent noise power spectra of the cavity (a) and the magnon (b) modes, at room temperature. The gray dashed lines indicate the threshold values defined through Eqs. (8) and (9). Panels (c) and (d) are the squeezed (blue) and anti-squeezed (red) quadrature variances of the cavity and magnon, respectively. Panel (e) illustrates the squeezing angle for the cavity (solid line) and magnon (dashed line). The parameters are the same as in Fig. 2, for which we have $gf_a^{lase}/\gamma_a^2 = 0.625$ and $gf_a^{comb}/\gamma_a^2 = 1.64$.

at which the magnon mode goes into the lasing phase. In the lasing phase, the magnon dynamics has a well-defined amplitude with two possible phases that are opposite to each other.[80] We note that for $4\Delta_a\Delta_s > \gamma_a\gamma_s$, the system shows bistability with downward threshold $f_a = |\gamma_s\Delta_a + \gamma_a\Delta_s|/(4g)$. Above the lasing threshold, the coherent magnon mode strongly couples the cavity and the magnon fluctuations. The strong coupling splits the resonance frequency. For the detunings $4\Delta_a(\Delta_a + 2\Delta_s) + \gamma_a(\gamma_a + 2\gamma_s) < 0$,[26] both the spectra exhibit narrowing, and at the threshold value of the drive $f_a \equiv f_a^{comb}$, where

$$f_a^{comb} = \sqrt{\frac{(\Delta_a\gamma_s + \gamma_a\Delta_s)^2}{16g^2} + \frac{1}{256g^2}\left(\frac{\gamma_a\gamma_s\left(\gamma_a^2 + 4\Delta_a^2\right)\left(4\Delta_a^2 + (\gamma_a + 2\gamma_s)^2\right)}{(\gamma_a + \gamma_s)^2(4\Delta_a(\Delta_a + 2\Delta_s) + \gamma_a(\gamma_a + 2\gamma_s))} - 2\gamma_a\gamma_s + 8\Delta_a\Delta_s\right)^2}, \tag{9}$$

the spectra are extremely narrow at two frequencies,

$$\omega_\pm = \pm\frac{1}{2}i\sqrt{\frac{\gamma_s\left(\gamma_a^2 + 4\Delta_a^2\right)}{(\gamma_a + \gamma_s)^2}} \times \sqrt{\frac{\gamma_s\left(\gamma_a^2 - 4\Delta_a^2 + 2\gamma_a\gamma_s\right) - 8\Delta_a\Delta_s(\gamma_a + \gamma_s)}{4\Delta_a(\Delta_a + 2\Delta_s) + \gamma_a(\gamma_a + 2\gamma_s)}}, \tag{10}$$

at which both the modes start to lase. At this threshold, the wave mixing between all the coherent components at the frequencies $\omega = \omega_-, 0, \omega_+$ gives rise to a comb of frequencies with an equal spacing of $|\omega_\pm|$.

We further investigate the quadrature fluctuations around the mean dynamics. From the linearized Langevin equation, we also obtain the quadrature spectral density $S_{XX}(\omega) = \int X(\omega)X(\omega')d\omega'$ for the quadrature operator $X(\phi) = (ce^{-i\phi} + c^\dagger e^{i\phi})/2$[20] and compute the mean-variance by integrating the spectrum, $\langle\Delta X(\phi)^2\rangle = \int_{-\infty}^{\infty} S_{XX}(\omega)d\omega$. Here, ϕ is the polar angle in phase-space, indicating the direction of X with $X(\phi = 0) = x$ and $X(\phi = \pi/2) = p$ being the position and momentum quadratures, respectively. The squeezed and anti-squeezed quadrature variances are shown in Figs. 3(c) and 3(d), respectively, and are determined by the phase ϕ, at which $\Delta X(\phi)$ is at its minimum or maximum. In Fig. 3(e), the angle ϕ represents the direction of squeezing corresponding to the minimum $\Delta X(\phi)$. At thermal equilibrium, the quadrature variance of the undriven system is independent of ϕ, i.e., $\langle\Delta X(\phi)^2\rangle = (\bar{n} + 1/2)/2$. Below the magnon lasing threshold, the parametric coupling squeezes the magnon mode. Above the lasing threshold, the strong cavity–magnon coupling also squeezes the cavity mode. With a proper choice of detunings, one can achieve squeezing in both the cavity and magnon modes $<(\bar{n}_j + 1/2)/2$.

Now, we investigate the fluctuations in the FC regime. Above the FC threshold, the linearization fails. Hence, we numerically solve the nonlinear Langevin equation (7) to quantify the quadrature variances. The quadrature spectral density and the phase-space probability distribution in the different regimes are shown in Fig. 4. When the system is in the FC regime, the dynamics exhibit limit cycles in the steady state with undefined phases ϕ. We observe an

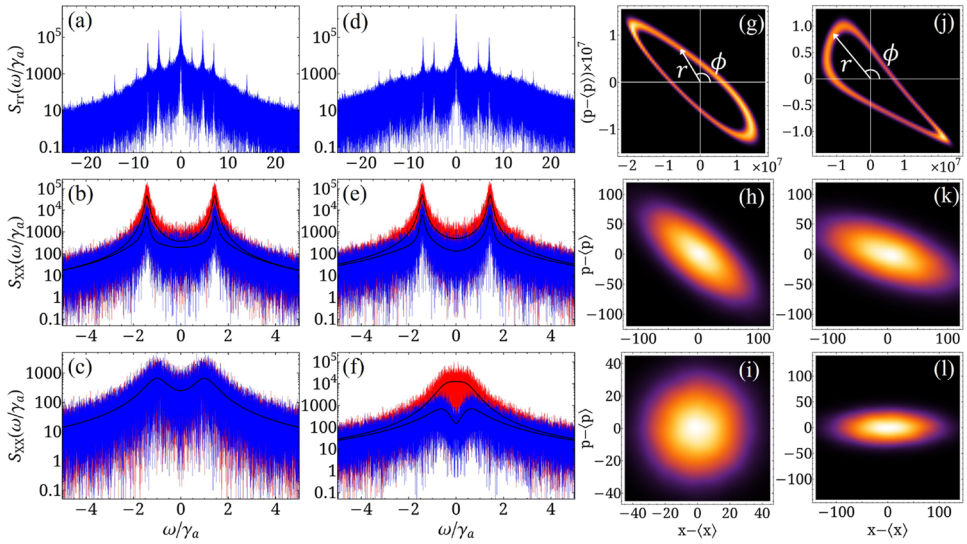

FIG. 4. Squeezed cavity-magnonic FC: the spectral density of the squeezed (blue) and anti-squeezed (red) quadratures for both cavity (a)–(c) and magnon modes (d)–(f) for different driving strengths: [FC regime: (a) and (d)] $f_a g/\gamma_a^2 = 2.0$, [above magnon lasing: (b) and (e)] $f_a g/\gamma_a^2 = 1.0$, and [below magnon lasing: (c) and (f)] $f_a g/\gamma_a^2 = 0.5$. The black lines represent the quadrature spectral density obtained after linearizing the nonlinear Langevin equation (7). In addition, this figure presents the corresponding phase-space probability distribution for both the cavity (g)–(i) and the magnon modes (j)–(l). Note that in panels (g) and (j), the fluctuations have been magnified by 10^4 to highlight the squeezing in $r(\phi)$. In order to be consistent with Fig. 2, we chose the same physical parameters.

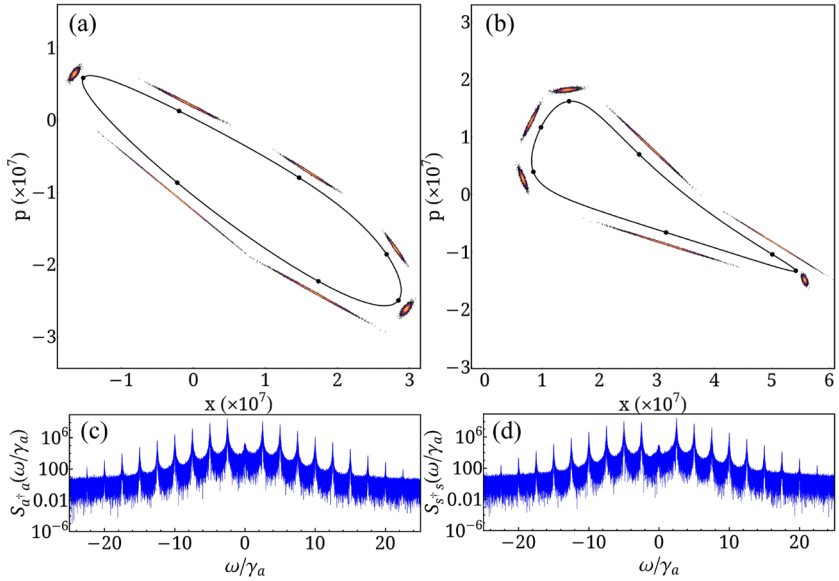

FIG. 5. Phase-locked phase-space distribution: In this figure, we plot a dynamical representation of the squeezing at some definite coordinates of phase-space (x, p, t) for both cavity (a) and magnon (b) modes. The black line is the mean phase-space trajectory, which is a limit cycle. The dots on the limit cycle are the phase-locked response at different time coordinates. We illustrate the magnified Q-function at different time points along the phase space trajectory. Panels (c) and (d) are the cavity and magnon power spectra, respectively. Here, we chose the same parameters as in Fig. 2 and used an input drive power of $P = 100$ mW and an additional weak injection power of 1 μW at a frequency of $\omega_d + 2.5$ MHz.

extremely slow phase diffusion over time, similar to the conventional lasers.[20,81] The slow phase diffusion or the long phase coherence leads to a substantially narrow comb spectrum, as shown in Figs. 4(a) and 4(b). In the limit of infinite time, the phase ϕ becomes completely uncertain [Figs. 4(g) and 4(j)]. However, the amplitude $r(\phi)$ is squeezed, and the squeezing depends on ϕ, as shown in Figs. 4(g) and 4(j). Although the generated FC has a long coherence time, the FC with a well-defined phase is more powerful. To solve this issue, we employed the so-called phase locking method to synchronize the FC.[81] This method involves injecting an additional weak driving signal into the system of the form $if_{weak}\left(a^\dagger e^{-i\omega_{lock}t} - ae^{i\omega_{lock}t}\right)$, where ω_{lock} is the frequency of the comb tooth adjacent to the central frequency. By implementing this technique, we successfully locked the phase and obtained the squeezing of the quadrature $\Delta X(\phi)$ along the trajectories in phase-space for both cavity and magnon modes, as shown in Fig. 5. This figure provides a visual representation in time of the squeezing phenomenon in the phase-space coordinates, shedding light on the intricate dynamics and correlations between position (x) and momentum (p). Observing the squeezing effects in both the cavity and magnon modes gives us insights into these systems' potential precision enhancement and control.

CONCLUSION

We have investigated the generation of cavity magnonic FCs in a driven cavity–magnon system that is parametrically coupled. By analyzing the mean dynamics and quadrature fluctuations, we find that when driven appropriately, the system exhibits squeezed lasing at multiple frequencies, developing a tunable FC in both the

microwave and magnon sub-systems. We have fully characterized the different regimes explored by this hybrid setup and obtained the threshold conditions under which the modes enter different phases. We have shown that the generated FCs are extremely narrow and have long coherence. We employed a phase-locking method to overcome the issue of phase diffusion and studied the dynamical squeezing of the quadratures Δx and Δp. Our findings demonstrate the potential of cavity-magnonic systems through the design of a room-temperature compact squeezed multi-frequency maser with potential applications in high-precision metrology and quantum information technology.

ACKNOWLEDGMENTS

We thank P. Puchenkov from the Scientific Computing and Data Analysis section of Research Support Division at OIST for the help and support. This work was supported by the funding from the Okinawa Institute of Science and Technology Graduate University. The authors have filed a provisional patent in Japan with filing No. 2023-201089.

AUTHOR DECLARATIONS

Conflict of Interest

The authors have no conflicts to disclose.

Author Contributions

A. Kani: Conceptualization (equal); Formal analysis (equal); Investigation (equal); Methodology (equal); Software (equal); Visualization (equal); Writing – original draft (equal); Writing – review & editing (lead). **M. Hatifi**: Conceptualization (equal); Formal analysis (equal); Investigation (equal); Methodology (equal); Software (equal); Visualization (equal); Writing – original draft (equal); Writing – review & editing (lead). **J. Twamley**: Conceptualization (equal); Formal analysis (equal); Investigation (equal); Methodology (equal); Project administration (equal); Resources (equal); Software (equal); Supervision (equal); Visualization (equal); Writing – original draft (equal); Writing – review & editing (equal).

DATA AVAILABILITY

The data that support the findings of this study are available within the article.

REFERENCES

[1] R. C. Shen, Y. P. Wang, J. Li, S. Y. Zhu, G. S. Agarwal, and J. Q. You, "Long-time memory and ternary logic gate using a multistable cavity magnonic system," Phys. Rev. Lett. **127**, 183202 (2021).
[2] H. Y. Yuan, P. Yan, S. Zheng, Q. Y. He, K. Xia, and M.-H. Yung, "Steady Bell state generation via magnon-photon coupling," Phys. Rev. Lett. **124**, 053602 (2020).
[3] S.-f. Qi and J. Jing, "Generation of Bell and Greenberger–Horne–Zeilinger states from a hybrid qubit-photon-magnon system," Phys. Rev. A **105**, 022624 (2022).
[4] J. Xu, C. Zhong, X. Han, D. Jin, L. Jiang, and X. Zhang, "Coherent gate operations in hybrid magnonics," Phys. Rev. Lett. **126**, 207202 (2021).
[5] X. Zhang, C.-L. Zou, N. Zhu, F. Marquardt, L. Jiang, and H. X. Tang, "Magnon dark modes and gradient memory," Nat. Commun. **6**, 8914 (2015).
[6] M. Goryachev, W. G. Farr, D. L. Creedon, Y. Fan, M. Kostylev, and M. E. Tobar, "High-cooperativity cavity QED with magnons at microwave frequencies," Phys. Rev. Appl. **2**, 054002 (2014).
[7] X. Zhang, C.-L. Zou, L. Jiang, and H. X. Tang, "Strongly coupled magnons and cavity microwave photons," Phys. Rev. Lett. **113**, 156401 (2014).
[8] Y. Tabuchi, S. Ishino, T. Ishikawa, R. Yamazaki, K. Usami, and Y. Nakamura, "Hybridizing ferromagnetic magnons and microwave photons in the quantum limit," Phys. Rev. Lett. **113**, 083603 (2014).
[9] U. L. Andersen, J. S. Neergaard-Nielsen, P. van Loock, and A. Furusawa, "Hybrid discrete- and continuous-variable quantum information," Nat. Phys. **11**, 713–719 (2015).
[10] U. L. Andersen, G. Leuchs, and C. Silberhorn, "Continuous-variable quantum information processing," Laser Photonics Rev. **4**, 337–354 (2010).
[11] A. Ourjoumtsev, R. Tualle-Brouri, J. Laurat, and P. Grangier, "Generating optical Schrodinger kittens for quantum information processing," Science **312**, 83–86 (2006).
[12] M. Zhang, B. Buscaino, C. Wang, A. Shams-Ansari, C. Reimer, R. Zhu, J. M. Kahn, and M. Lončar, "Broadband electro-optic frequency comb generation in a lithium niobate microring resonator," Nature **568**, 373–377 (2019).
[13] O. Pinel, P. Jian, R. M. de Arajo, J. Feng, B. Chalopin, C. Fabre, and N. Treps, "Generation and characterization of multimode quantum frequency combs," Phys. Rev. Lett. **108**, 083601 (2012).
[14] C. Reimer, M. Kues, P. Roztocki, B. Wetzel, F. Grazioso, B. E. Little, S. T. Chu, T. Johnston, Y. Bromberg, L. Caspani, D. J. Moss, and R. Morandotti, "Generation of multiphoton entangled quantum states by means of integrated frequency combs," Science **351**, 1176–1180 (2016).
[15] A. E. Dunlop, E. H. Huntington, C. C. Harb, and T. C. Ralph, "Generation of a frequency comb of squeezing in an optical parametric oscillator," Phys. Rev. A **73**, 013817 (2006).
[16] Z. Yang, M. Jahanbozorgi, D. Jeong, S. Sun, O. Pfister, H. Lee, and X. Yi, "A squeezed quantum microcomb on a chip," Nat. Commun. **12**, 4781 (2021).
[17] M. Kues, C. Reimer, J. M. Lukens, W. J. Munro, A. M. Weiner, D. J. Moss, and R. Morandotti, "Quantum optical microcombs," Nat. Photonics **13**, 170–179 (2019).
[18] T. Fortier and E. Baumann, "20 years of developments in optical frequency comb technology and applications," Commun. Phys. **2**, 153–216 (2019).
[19] U. L. Andersen, T. Gehring, C. Marquardt, and G. Leuchs, "30 years of squeezed light generation," Phys. Scr. **91**, 053001 (2016).
[20] C. Sánchez Muñoz and D. Jaksch, "Squeezed lasing," Phys. Rev. Lett. **127**, 183603 (2021).
[21] Y. Cai, J. Roslund, V. Thiel, C. Fabre, and N. Treps, "Quantum enhanced measurement of an optical frequency comb," npj Quantum Inf. **7**, 82 (2021).
[22] B.-H. Wu, R. N. Alexander, S. Liu, and Z. Zhang, "Quantum computing with multidimensional continuous-variable cluster states in a scalable photonic platform," Phys. Rev. Res. **2**, 023138 (2020).
[23] L. Zhang, C. Cui, J. Yan, Y. Guo, J. Wang, and L. Fan, "On-chip parallel processing of quantum frequency comb," npj Quantum Inf. **9**, 57 (2023).
[24] N. C. Menicucci, S. T. Flammia, and O. Pfister, "One-way quantum computing in the optical frequency comb," Phys. Rev. Lett. **101**, 130501 (2008).
[25] A. Ganesan, C. Do, and A. Seshia, "Phononic frequency comb via intrinsic three-wave mixing," Phys. Rev. Lett. **118**, 033903 (2017).
[26] Z. Qi, C. R. Menyuk, J. J. Gorman, and A. Ganesan, "Existence conditions for phononic frequency combs," Appl. Phys. Lett. **117**, 5–10 (2020).
[27] J. S. Ochs, D. K. Boneß, G. Rastelli, M. Seitner, W. Belzig, M. I. Dykman, and E. M. Weig, "Frequency comb from a single driven nonlinear nanomechanical mode," Phys. Rev. X **12**, 41019 (2022).
[28] J. Sun, S. Yu, H. Zhang, D. Chen, X. Zhou, C. Zhao, D. D. Gerrard, R. Kwon, G. Vukasin, D. Xiao, T. W. Kenny, X. Wu, and A. Seshia, "Generation and evolution of phononic frequency combs via coherent energy transfer between mechanical modes," Phys. Rev. Appl. **19**, 014031 (2023).
[29] L. Caspani, C. Reimer, M. Kues, P. Roztocki, M. Clerici, B. Wetzel, Y. Jestin, M. Ferrera, M. Peccianti, A. Pasquazi, L. Razzari, B. E. Little, S. T. Chu, D. J. Moss, and R. Morandotti, "Multifrequency sources of quantum correlated photon pairs

on-chip: A path toward integrated quantum frequency combs," Nanophotonics **5**, 351–362 (2016).
[30]J. Shin, Y. Ryu, M. A. Miri, S. B. Shim, H. Choi, A. Alù, J. Suh, and J. Cha, "On-chip microwave frequency combs in a superconducting nanoelectromechanical device," Nano Lett. **22**, 5459–5465 (2022).
[31]A. Keşkekler, H. Arjmandi-Tash, P. G. Steeneken, and F. Alijani, "Symmetry-breaking-induced frequency combs in graphene resonators," Nano Lett. **22**, 6048–6054 (2022).
[32]M. Wang, C. Kong, Z.-Y. Sun, D. Zhang, Y.-Y. Wu, and L.-L. Zheng, "Nonreciprocal high-order sidebands induced by magnon Kerr nonlinearity," Phys. Rev. A **104**, 033708 (2021).
[33]Z. Wang, H. Y. Yuan, Y. Cao, Z.-X. Li, R. A. Duine, and P. Yan, "Magnonic frequency comb through nonlinear magnon-skyrmion scattering," Phys. Rev. Lett. **127**, 037202 (2021).
[34]Z. Wang, H. Y. Yuan, Y. Cao, and P. Yan, "Twisted magnon frequency comb and penrose superradiance," Phys. Rev. Lett. **129**, 107203 (2022).
[35]T. Hula, K. Schultheiss, F. J. T. Gonçalves, L. Körber, M. Bejarano, M. Copus, L. Flacke, L. Liensberger, A. Buzdakov, A. Kákay, M. Weiler, R. Camley, J. Fassbender, and H. Schultheiss, "Spin-wave frequency combs," Appl. Phys. Lett. **121**, 112404 (2022).
[36]Z.-X. Liu, B. Wang, H. Xiong, and Y. Wu, "Magnon-induced high-order sideband generation," Opt. Lett. **43**, 3698 (2018).
[37]Z.-X. Liu and Y.-Q. Li, "Optomagnonic frequency combs," Photonics Res. **10**, 2786 (2022).
[38]H. Xiong, "Magnonic frequency combs based on the resonantly enhanced magnetostrictive effect," Fundam. Res. **3**, 8–14 (2023).
[39]Z.-X. Liu, J. Peng, and H. Xiong, "Generation of magnonic frequency combs via a two-tone microwave drive," Phys. Rev. A **107**, 053708 (2023).
[40]G.-T. Xu, M. Zhang, Y. Wang, Z. Shen, G.-C. Guo, and C.-H. Dong, "Magnonic frequency comb in the magnomechanical resonator," Phys. Rev. Lett. **131**, 243601 (2023).
[41]Z.-B. Yang, H. Jin, J.-W. Jin, J.-Y. Liu, H.-Y. Liu, and R.-C. Yang, "Bistability of squeezing and entanglement in magnonics," Phys. Rev. Res. **3**, 023126 (2021).
[42]J. Li, S.-Y. Zhu, and G. S. Agarwal, "Squeezed states of magnons and phonons in cavity magnomechanics," Phys. Rev. A **99**, 021801 (2019).
[43]S. Huang, L. Deng, and A. Chen, "Squeezed states of magnons and phonons in a cavity magnomechanical system with a microwave parametric amplifier," Ann. Phys. **535**, 2300095 (2023).
[44]M. Asjad, J. Li, S.-Y. Zhu, and J. You, "Magnon squeezing enhanced ground-state cooling in cavity magnomechanics," Fundam. Res. **3**, 3–7 (2023).
[45]M.-S. Ding, L. Zheng, Y. Shi, and Y.-J. Liu, "Magnon squeezing enhanced entanglement in a cavity magnomechanical system," J. Opt. Soc. Am. B **39**, 2665 (2022).
[46]T.-X. Lu, X. Xiao, L.-S. Chen, Q. Zhang, and H. Jing, "Magnon-squeezing-enhanced slow light and second-order sideband in cavity magnomechanics," Phys. Rev. A **107**, 063714 (2023).
[47]J. Roslund, R. M. de Araújo, S. Jiang, C. Fabre, and N. Treps, "Wavelength-multiplexed quantum networks with ultrafast frequency combs," Nat. Photonics **8**, 109–112 (2014).
[48]A. Bienfait, P. Campagne-Ibarcq, A. H. Kiilerich, X. Zhou, S. Probst, J. J. Pla, T. Schenkel, D. Vion, D. Esteve, J. J. L. Morton, K. Moelmer, and P. Bertet, "Magnetic resonance with squeezed microwaves," Phys. Rev. X **7**, 041011 (2017).
[49]R. Assouly, R. Dassonneville, T. Peronnin, A. Bienfait, and B. Huard, "Quantum advantage in microwave quantum radar," Nat. Phys. **19**, 1418–1422 (2023).
[50]S. Pogorzalek, K. G. Fedorov, M. Xu, A. Parra-Rodriguez, M. Sanz, M. Fischer, E. Xie, K. Inomata, Y. Nakamura, E. Solano, A. Marx, F. Deppe, and R. Gross, "Secure quantum remote state preparation of squeezed microwave states," Nat. Commun. **10**, 2604 (2019).
[51]K. G. Fedorov, M. Renger, S. Pogorzalek, R. Di Candia, Q. Chen, Y. Nojiri, K. Inomata, Y. Nakamura, M. Partanen, A. Marx, R. Gross, and F. Deppe, "Experimental quantum teleportation of propagating microwaves," Sci. Adv. **7**, eabk0891 (2021).
[52]H. Suhl, "The theory of ferromagnetic resonance at high signal powers," J. Phys. Chem. Solids **1**, 209–227 (1957).
[53]E. Schlömann, J. J. Green, and U. Milano, "Recent developments in ferromagnetic resonance at high power levels," J. Appl. Phys. **31**, S386–S395 (1960).
[54]B. Heinz, M. Mohseni, A. Lentfert, R. Verba, M. Schneider, B. Lägel, K. Levchenko, T. Brächer, C. Dubs, A. V. Chumak, and P. Pirro, "Parametric generation of spin waves in nanoscaled magnonic conduits," Phys. Rev. B **105**, 144424 (2022).
[55]T. Brächer, P. Pirro, and B. Hillebrands, "Parallel pumping for magnon spintronics: Amplification and manipulation of magnon spin currents on the micron-scale," Phys. Rep. **699**, 1–34 (2017).
[56]P. Krivosik and C. E. Patton, "Hamiltonian formulation of nonlinear spin-wave dynamics: Theory and applications," Phys. Rev. B **82**, 184428 (2010).
[57]H. G. Bauer, P. Majchrak, T. Kachel, C. H. Back, and G. Woltersdorf, "Nonlinear spin-wave excitations at low magnetic bias fields," Nat. Commun. **6**, 8274 (2015).
[58]R. Dreyer, A. F. Schäffer, H. G. Bauer, N. Liebing, J. Berakdar, and G. Woltersdorf, "Imaging and phase-locking of non-linear spin waves," Nat. Commun. **13**, 4939 (2022).
[59]F. Guo, L. M. Belova, and R. D. McMichael, "Parametric pumping of precession modes in ferromagnetic nanodisks," Phys. Rev. B **89**, 104422 (2014).
[60]T. Makiuchi, T. Hioki, Y. Shimazu, Y. Oikawa, N. Yokoi, S. Daimon, and E. Saitoh, "Parametron on magnetic dot: Stable and stochastic operation," Appl. Phys. Lett. **118**, 022402 (2021).
[61]H. Ulrichs, V. E. Demidov, S. O. Demokritov, and S. Urazhdin, "Parametric excitation of eigenmodes in microscopic magnetic dots," Phys. Rev. B **84**, 094401 (2011).
[62]A. A. Serga, A. V. Chumak, and B. Hillebrands, "YIG magnonics," J. Phys. D: Appl. Phys. **43**, 264002 (2010).
[63]L. R. Walker, "Magnetostatic modes in ferromagnetic resonance," Phys. Rev. **105**, 390–399 (1957).
[64]P. C. Fletcher and R. O. Bell, "Ferrimagnetic resonance modes in spheres," J. Appl. Phys. **30**, 687–698 (1959).
[65]A. Leo, A. G. Monteduro, S. Rizzato, L. Martina, and G. Maruccio, "Identification and time-resolved study of ferrimagnetic spin-wave modes in a microwave cavity in the strong-coupling regime," Phys. Rev. B **101**, 014439 (2020).
[66]J. A. Haigh, N. J. Lambert, S. Sharma, Y. M. Blanter, G. E. W. Bauer, and A. J. Ramsay, "Selection rules for cavity-enhanced Brillouin light scattering from magnetostatic modes," Phys. Rev. B **97**, 214423 (2018).
[67]R. G. E. Morris, A. F. van Loo, S. Kosen, and A. D. Karenowska, "Strong coupling of magnons in a YIG sphere to photons in a planar superconducting resonator in the quantum limit," Sci. Rep. **7**, 11511 (2017).
[68]J. Cho, S. Miwa, K. Yakushiji, S. Tamaru, H. Kubota, A. Fukushima, S. Fujimoto, E. Tamura, C.-Y. You, S. Yuasa, and Y. Suzuki, "Spin-wave eigenmodes in single disk-shaped FeB nanomagnet," Phys. Rev. B **94**, 184411 (2016).
[69]C. Gonzalez-Ballestero, D. Hümmer, J. Gieseler, and O. Romero-Isart, "Theory of quantum acoustomagnonics and acoustomechanics with a micromagnet," Phys. Rev. B **101**, 125404 (2020).
[70]A. Kani, F. Quijandría, and J. Twamley, "Magnonic Einstein–de Haas effect: Ultrafast rotation of magnonic microspheres," Phys. Rev. Lett. **129**, 257201 (2022).
[71]Y. S. Ihn, S.-Y. Lee, D. Kim, S. H. Yim, and Z. Kim, "Coherent multimode conversion from microwave to optical wave via a magnon-cavity hybrid system," Phys. Rev. B **102**, 064418 (2020).
[72]A. Osada, "Sustainability (Switzerland)," Ph.D. thesis, University of Tokyo, 2017.
[73]G. Emdi, T. Hioki, K. Hoshi, and E. Saitoh, "Electrical detection of parallel parametric amplification and attenuation in a $Y_3Fe_5O_{12}$/Pt bilayer disk," Phys. Rev. B **108**, L140410 (2023).
[74]Y.-P. Wang, G.-Q. Zhang, D. Zhang, X.-Q. Luo, W. Xiong, S.-P. Wang, T.-F. Li, C.-M. Hu, and J. Q. You, "Magnon Kerr effect in a strongly coupled cavity-magnon system," Phys. Rev. B **94**, 224410 (2016).
[75]Y.-P. Wang, G.-Q. Zhang, D. Zhang, T.-F. Li, C.-M. Hu, and J. Q. You, "Bistability of cavity magnon polaritons," Phys. Rev. Lett. **120**, 057202 (2018).

[76]G. Zhang, Y. Wang, and J. You, "Theory of the magnon Kerr effect in cavity magnonics," Sci. China: Phys., Mech. Astron. **62**, 987511 (2019).
[77]V. Zakharov and V. L'vov, "Onset of turbulence during parametric excitation of waves," Sov. Phys. JETP **33**, 1113 (1971) http://jetp.ras.ru/cgi-bin/dn/e_033_06_1113.pdf.
[78]B. Zare Rameshti, S. Viola Kusminskiy, J. A. Haigh, K. Usami, D. Lachance-Quirion, Y. Nakamura, C.-M. Hu, H. X. Tang, G. E. Bauer, and Y. M. Blanter, "Cavity magnonics," Phys. Rep. **979**, 1–61 (2022).
[79]H. Yuan, Y. Cao, A. Kamra, R. A. Duine, and P. Yan, "Quantum magnonics: When magnon spintronics meets quantum information science," Phys. Rep. **965**, 1–74 (2022).
[80]Z. Wang, M. Pechal, E. A. Wollack, P. Arrangoiz-Arriola, M. Gao, N. R. Lee, and A. H. Safavi-Naeini, "Quantum dynamics of a few-photon parametric oscillator," Phys. Rev. X **9**, 021049 (2019).
[81]B. Yao, Y. S. Gui, J. W. Rao, Y. H. Zhang, W. Lu, and C.-M. Hu, "Coherent microwave emission of gain-driven polaritons," Phys. Rev. Lett. **130**, 146702 (2023).